

Synthesis and characterization of Fe:MgZnO/AC as a prospective high photocatalytic material

M. S. Çevik^a, S. Horoz^b, O. Baytar^c, Ö. Şahin^c, A. Ekinci^{d,*}

^a*Siirt University, Institute of Science and Technology, Siirt, 56100, Turkey*

^b*Siirt University, Faculty of Engineering, Department of Electrical and Electronics Engineering, Siirt, Turkey, 56100*

^c*Siirt University, Faculty of Engineering, Department of Chemical Engineering, Siirt, Turkey, 56100*

^d*Department of Occupational Health and Safety, Siirt School of Health, Siirt University, Siirt, Turkey, 56100*

The motivation of our current study is to carry out photocatalytic degradation experiments of methylene blue in the presence of Fe doped MgZnO/AC (Fe:MgZnO/AC) and MgZnO/AC catalysts and thus to examine the effect of the Fe-dopant metal on the photocatalytic activity of the catalysts. In this context, both catalysts (MgZnO/AC and Fe:MgZnO/AC) are synthesized by hydrothermal technique. Structural (XRD analysis) and optical (UV-Vis) properties of the synthesized catalysts are discussed. How the Fe-dopant metal affects the crystallite size and energy band gap of the MgZnO/AC catalyst is examined and the experimental data obtained are interpreted.

(Received February 21, 2021; Accepted June 2, 2021)

Keywords: Catalyst, Characterization, Doped material, Metal oxide, Photocatalytic

1. Introduction

Organic pollutants cause water pollution, which is an important environmental problem, due to the rapid development of the global industry [1, 2]. The main sources of synthetic organic pollutants that show their presence in the natural environment stand out as the textile, leather and food industries [3-5]. The damages that these pollutants cause to human health are well known to humanity [6].

Methylene blue, which belongs to the group of anionic azo dyes, is resistant to classical biological treatment and does not decompose under normal conditions [7-10]. Reverse osmosis, coagulation and adsorption are some of the methods used to purify or remove methylene blue from the aqueous environment. One of the most important disadvantages of these methods is that they do not transform the dyestuff into harmless compounds [11, 12]. In this context, scientific techniques were needed to develop new methods for the efficient removal of methylene blue from aqueous solutions. In recent years, the photocatalytic degradation approach used to completely mineralize dyes in wastewater has become of great importance [13-15].

ZnO semiconductor materials, which have advantages such as superior photocatalytic properties, low toxicity and chemical stability, are among the most effective catalysts used in photocatalytic degradation experiments. ZnO, which can only be excited under UV irradiation, has a wide energy band range (3.37 eV) [16-19]. The photocatalytic activity of ZnO under visible light is limited since sunlight contains approximately 5% UV light. Another striking negative effect is that the recombination time of the photogenerated electron-hole pair occurs in a very short time [20, 21].

This situation limits the photodegradation reaction. Alternative ways have been tried to overcome these disadvantages. One of them modifies ZnO using dopants (metal or non-metal) [22-24]. Studies on doped ZnO catalysts show that doped ZnO has higher photocatalytic activity compared to pure ZnO [25, 26]. It has been reported that the doped ZnO catalyst has an effective

* Corresponding author: aekinci80@gmail.com

absorption property under visible light and prevents photogenerated electron-hole recombination [27]. In this context, it will be useful to examine both optical and photocatalytic properties of different doped ZnO catalysts.

One of the factors that limits the practical industrial application of the ZnO catalyst is that the recovery of ZnO from treated wastewater is difficult. Effective approaches to solve this problem are of great importance. One of these approaches is the use of porous structures as support material for catalysts. Activated carbon (AC) has attracted great attention in this regard due to its large specific surface area and rich functional groups as a support material [28-31]. In the study, it was emphasized that the AC supported ZnO catalyst used was easily removed from the solution during wastewater treatment and that the same catalyst could be reused in an effective treatment process. Although there are many experimental studies on AC supported ZnO catalysts, no study has been found by photocatalytic degradation of methylene blue in the presence of AC supported Fe-doped ZnMgO (Fe:ZnMgO/AC) catalysts. Therefore, it would be valuable to study the photocatalytic activity behavior of the ZnMgO catalyst in the presence of both support material (AC) and doped metal (Fe).

In the present study, Fe:ZnMgO/AC catalysts were synthesized using the classical hydrothermal method. Photocatalytic degradation experiments of methylene blue in the presence of these catalysts were carried out and the results obtained were discussed.

2. Experimental study

To synthesize the MgZnO/AC catalyst, 1.1 g of zinc acetate, 0.008 g of magnesium nitrate and 10% by weight of activated carbon (AC) were added and dissolved at room temperature with stirring. Then, aqueous NaOH solution (0.3 M) was added dropwise to the solution with stirring at room temperature until the pH of the solution was 11. The resulting solution was stirred for half an hour. It was then transferred into a 100 mL autoclave. The autoclave was kept at 200 °C for 6 hours in the oven. The solution in the autoclave was cooled to room temperature, filtered with filter paper, washed three times with distilled water to remove unreacted reagents, and then dried at 60 °C for 6 hours.

To synthesize the Fe:MgZnO/AC catalyst, 0.002 g of iron nitrate was added to the above mixture and the same process was repeated.

To study the degradation of methylene blue solution in the presence of a catalyst, photocatalytic measurements were carried out using a 500 W Xe lamp as the visible light source. Xe lamp power was kept at 500 W and preserved an overall irradiation strength of 350 W/m² across the tests. The catalyst was transferred to the solution of methylene blue. The solution was consistently stirred and held for 1h in the dark to permit an adsorption-desorption balance between methylene blue and the catalyst. The suspension was subsequently displayed under visible light to eliminate methylene blue. Each sample was subsequently extracted after degradation test to avoid catalyst for examination.

XRD (Rigaku X-ray diffractometer), SEM, EDX (JEOL JSM 5800) and UV-Vis absorption spectra (Perkin Elmer Lambda 2 spectrometer) measurements were carried out to examine the structural, morphological and optical properties of catalyst.

3. Results and discussion

3.1. Powder XRD analysis of Fe:MgZnO/AC catalyst

XRD measurements were made to determine the crystal structure of the synthesized catalysts (MgZnO/AC and Fe:MgZnO/AC). The diffraction peaks of MgZnO/AC and Fe:MgZnO/AC in the XRD patterns (Fig. 1) were indexed and the wurtzite structure was assigned to the MgZnO phase with a hexagonal crystal system belonging to the P63mc space group, which matches well with (PDF NO. 01-076-8936). XRD patterns show peaks at $2\theta = 31.83, 34.51, 36.58, 47.64, 56.71, \text{ and } 62.99$ and were, respectively, indexed to the (200), (002), (101), (102), (110),

and (103) planes. No secondary phases such as MgO and Fe₂O₃ were observed even for the MgZnO/AC and Fe:MgZnO/AC catalysts with magnesium and iron contents. Inclusion of Fe³⁺ in the MgZnO lattice may occupy the substitution site or the intermediate region. In this case, Fe³⁺ ions predominantly occupy the intermediate regions causing an increase in lattice parameters and a shift of the diffraction peaks of the doped catalysts towards the smaller 2θ, as indicated in Fig. 1.

The average crystallite size for MgZnO/AC and Fe:MgZnO/AC catalysts was calculated from the FWHM of the diffraction peaks by the Debye-Scherrer equation [32]:

$$d_c = \frac{k \cdot \lambda}{\beta \cos \theta} \quad (1)$$

where d_c (nm) is the crystallite size, k is the shape factor with a value close to unity (0.9), λ (1.540564 Å) is the wavelength of monochromatic Cu-K_α radiations, β is the full width at half maximum (FWHM in radians) of the respective peaks and θ is the diffraction angle.

The average crystallite size for MgZnO/AC and Fe:MgZnO/AC catalysts were found as 11.62 and 12.87 nm, respectively. Possible cause for the increase in crystallite size: The addition of Fe³⁺ ions into the host lattice causes the expansion of the unit cell resulting in occurrence of tensile stress responsible for shifting of peaks towards the lower angles.

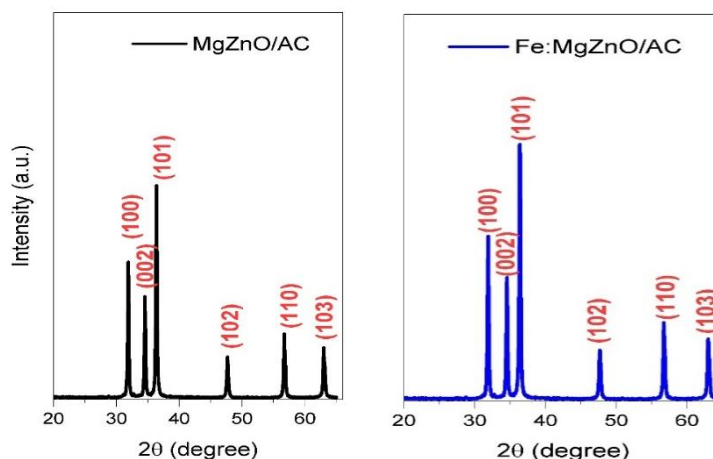


Fig. 1. Recorded XRD patterns of MgZnO/AC and Fe:MgZnO/AC catalysts

3.2. EDX analysis of Fe:MgZnO/AC catalysts

Energy dispersive x-ray spectroscopy (EDX) measurements were performed to determine the composition of the synthesized Fe:MgZnO/AC catalyst, in other words, to investigate the presence of elements zinc (Zn), magnesium (Mg), oxygen (O) and iron (Fe) in the sample. Fig. 2 shows the typical EDX spectrum of Fe³⁺ doped MgZnO nanoparticles consisting of Zn, Mg, O and Fe, showing no impurity peaks, and Table 1 describes the atomic and weight percentage of the elements found in the prepared catalyst. The EDX spectrum effectively supports the doping of Fe³⁺ to the MgZnO parent matrix.

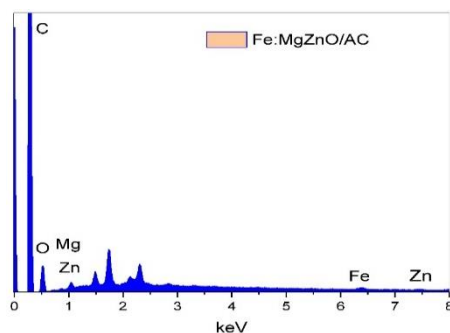


Fig. 2. The EDX spectra of Fe:MgZnO/AC catalyst

Table 1. Atomic and weight percentage of elements present in Fe:MgZnO/AC catalyst

Element	Weight (%)	Atomic (%)
Oxygen (O)	8.21	25.16
Magnesium (Mg)	0.15	0.27
Carbon (C)	84.32	69.18
Zinc (Zn)	4.12	4.82
Iron (Fe)	3.20	0.57

3.3. SEM analysis of Fe:MgZnO/AC catalyst

The morphology and textural properties of the Fe:MgZnO/AC catalyst were investigated using SEM analysis. As seen in Fig. 3, the Fe:MgZnO/AC catalyst exhibits solid form in the 5–10 μm range. It should also be noted that Fe:MgZnO effectively coated the catalyst to the surface of the AC structure, even if not homogeneously. The rough surface of the Fe:MgZnO/AC catalyst causes a high degree of pores. The presence of these pores provided the mass transfer channel of products and reactants in photocatalytic experiments.

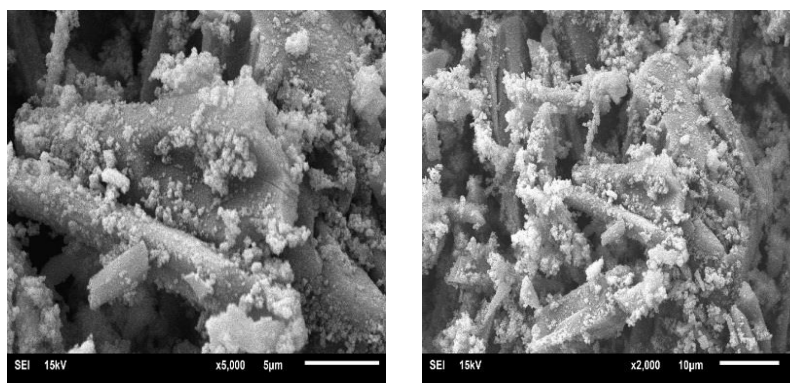


Fig. 3. TEM micrographs of Fe:MgZnO/AC catalyst.

3.4. UV–visible spectroscopy of Fe:MgZnO/AC catalyst

Fig. 4 reveals the Tauc's plot for the determination of direct and indirect optical bandgap of MgZnO/AC and Fe:MgZnO/AC catalysts [33]. These curves were plotted by the use of

$$(ahv) = A(hv - E_g)^n \quad (2)$$

where E_g is the optical bandgap, hv is the incident photon energy, α is the absorption coefficient. By plotting (ahv) against photon energy (hv) and extrapolating the linear portion of the plot, the bandgap was evaluated. Table 2 indicates the optical bandgap values for MgZnO/AC and Fe:MgZnO/AC catalysts. It can be observed that catalyst with concentration of Fe^{3+} experience an

increase in bandgap. For Fe:MgZnO/AC catalyst, the variation in bandgap could be due to the structural disorder caused by the incorporation of Fe³⁺ ions [34].

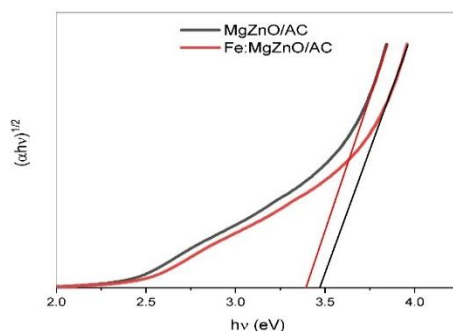


Fig. 4. Bandgap energy estimation by Tauc plots for MgZnO/AC and Fe:MgZnO/AC catalysts.

Table 2. Bandgap energy values of MgZnO/AC and Fe:MgZnO/AC catalysts.

Catalysts	E _g (eV)
MgZnO/AC	3.32
Fe:MgZnO/AC	3.46

3.5. Photocatalytic activity of Fe:MgZnO/AC catalyst

The graph of time vs photocatalytic degradation of methylene blue in the presence of MgZnO/AC and Fe:MgZnO/AC catalysts is given in Fig. 5. The parameters used in the photocatalytic test are methylene blue concentration (20 ppm) and catalyst amount (10 mg). When the two catalysts were compared, it was clearly observed that the photocatalytic activity of the Fe:MgZnO/AC catalyst was higher than that of the MgZnO/AC catalyst. The photocatalytic degradation reaction of methylene blue was completed in 15 minutes in the presence of Fe:MgZnO/AC catalyst, while the same reaction was completed in 20 minutes in the presence of MgZnO/AC catalyst. Moreover, the photocatalytic degradation percentage (%) of MgZnO/AC and Fe:MgZnO/AC catalysts was 93.10 and 97.59, respectively, when the 15th minute of the reaction was taken as reference. As a result, Fe dopant metal increased the photocatalytic activity of MgZnO/AC catalyst. This could be due to the substitution of Fe³⁺ ions in the MgO crystal system, which can get oxidized to Fe³⁺ by discharging electrons which can encourage lead to arrangement of superoxide radicals (O₂⁻) by responding with adsorbed O₂. The oxidized Fe³⁺ species can act as electron scavenger or acceptor to trap photoexcited electrons from conduction band (CB) of MgO and subsequently reduced to Fe³⁺. Hence, the electron (e⁻)-hole (h⁺) recombination can be enormously decreased driving to improved photocatalytic performance [35].

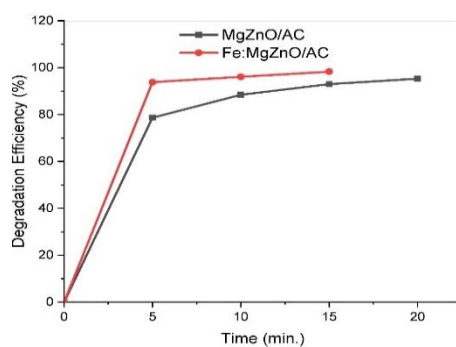


Fig. 5. Photocatalytic degradation of photocatalytic degradation of methylene blue in the presence of MgZnO/AC and Fe:MgZnO/AC catalysts.

In the presence of Fe:MgZnO/AC catalyst, the photocatalytic degradation kinetics of methylene blue was examined with the first and second-order kinetic model. First and second-order kinetic model equations are given below.

$$-\ln\left(\frac{C_t}{C_o}\right) = k_1 \cdot t \quad (3)$$

$$\frac{1}{C_t} - \frac{1}{C_o} = k_2 \cdot t \quad (4)$$

where C_t : solution concentration at the time t (mg/L), C_o : initial solution concentration (mg /L), k_1 : the first order adsorption rate constant (min^{-1}), k_2 : the second-order adsorption rate constant (min^{-1}), t : adsorption time (min.)

The plots obtained from the above equations for the first and second-order kinetic model are given in Fig. 6 and Fig. 7, respectively.

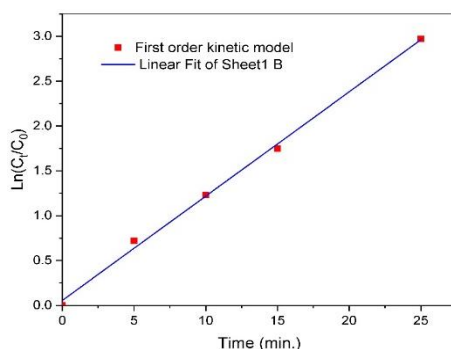


Fig. 6. The first-order kinetic model for the photocatalytic degradation of methylene blue in the presence of Fe:MgZnO/AC catalyst.

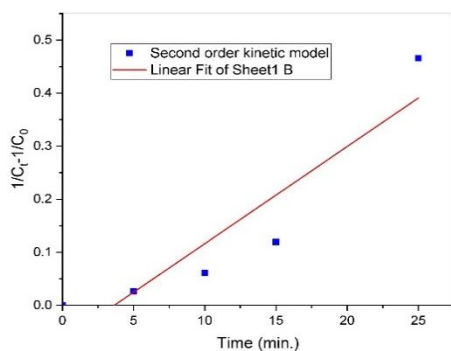


Fig. 7. The second-order kinetic model for the photocatalytic degradation of methylene blue in the presence of Fe:MgZnO/AC catalyst.

The regression coefficients (R^2) of Fe:MgZnO/AC catalyst were determined as 0.99 and 0.85, respectively. According to the regression coefficient, it was observed that the photocatalytic degradation kinetics of methylene blue fits the first order kinetic model better.

4. Conclusions

Our main purpose in the present study was to examine how the photocatalytic, crystallite size and energy band gap of the MgZnO/AC catalyst (Fe:MgZnO/AC) change in the presence of Fe-doped metal. Photocatalytic degradation experiments of methylene blue were carried out in the presence of MgZnO/AC and Fe:MgZnO/AC catalysts and the photocatalytic degradation (%) of Fe:MgZnO/AC catalyst in 15 seconds was 97.59, while this value was 93.10 for the MgZnO/AC catalyst. It showed that the Fe dopant metal increases the photocatalytic activity of the MgZnO/AC catalyst significantly. In the kinetic study, it was determined that the photocatalytic degradation of methylene blue in the presence of Fe:MgZnO/AC catalyst was suitable for first-order kinetic model.

In addition to the photocatalytic study, the crystallite size and energy band gap value of Fe:MgZnO/AC catalyst were found as 12.87 nm and 3.46 nm, respectively. It has been concluded that a wide energy band range and low size crystallite size positively affect the photocatalytic activity of Fe:MgZnO/AC catalyst.

Acknowledgments

The authors are grateful to the Research Foundation of Siirt University for financial support under project 2019-SIÜFEB-019.

References

- [1] N. Daneshvar, M. Ayazloo, A. Khataee, M. Pourhassan, *Bioresource technology* **98**, 1182 (2007).
- [2] M. Erdoğan, S. Horoz, *Journal of Chemical Research* **45** 212 (2021).
- [3] S. Kutluay, O. Baytar, Ö. Şahin, A. Arran, *European Journal of Technique* **10**, 142 (2020).
- [4] A. Mohammadi, M. Ghaedi, M.M. Sabzehmeidani, *Desalination and Water Treatment* **127**, 353 (2018).
- [5] A. Regti, M.R. Laamari, S.-E. Stiriba, M. El Haddad, *Microchemical Journal* **130**, 136 (2017).
- [6] M.M. Higgins, M.T. González, J. Rojas, *Radiation Physics and Chemistry* **156**, 80 (2019).
- [7] S. Horoz, O. Baytar, O. Sahin, H. Kilicvuran, *Journal of Materials Science: Materials in Electronics* **29**, 1010 (2018).
- [8] E.N. Zare, A. Motahari, M. Sillanpää, *Environmental research* **162**, 195 (2018).
- [9] I. Altuntas, M.N. Kocak, G. Yolcu, H.F. Budak, A.E. Kasapoğlu, S. Horoz, E. Gür, I. Demir, *Materials Science in Semiconductor Processing* **127**, 105733 (2021).
- [10] M. Erdoğan, *Journal of Molecular Structure* **1232**, 130056 (2021).
- [11] Y. He, Y. Xiang, Y. Zhou, Y. Yang, J. Zhang, H. Huang, C. Shang, L. Luo, J. Gao, L. Tang, *Environmental research* **164**, 301 (2018).
- [12] S. Liu, C. Gunawan, N. Barraud, S.A. Rice, E.J. Harry, R. Amal, *Environmental science & technology* **50**, 8976 (2016).
- [13] N. Bulut, O. Baytar, Ö. Şahin, S. Horoz, *Journal of Ovonic Research* **15**, 150 (2019).
- [14] S. Patnaik, S. Martha, S. Acharya, K. Parida, *Inorganic Chemistry Frontiers* **3**, 347 (2016).
- [15] I. Demir, H. Li, Y. Robin, R. McClintock, S. Elagoz, M. Razeghi, *Journal of Physics D: Applied Physics* **51**, 085104 (2018).
- [16] Q. Wan, T. Wang, J. Zhao, *Applied Physics Letters* **87**, 083105 (2005).
- [17] Y. Zheng, C. Chen, Y. Zhan, X. Lin, Q. Zheng, K. Wei, J. Zhu, *The Journal of Physical Chemistry C* **112**, 10777 (2008).
- [18] I. Demir, I. Altuntas, A.E. Kasapoğlu, S. Mobtakeri, E. Gür, S. Elagoz, *Semiconductors* **52**, 2038 (2018).
- [19] A. Kapicioglu, *Journal of Thermal Analysis and Calorimetry* (2021).
- [20] U. Alver, T. Kılınç, E. Bacaksız, S. Nezir, *Materials Science and Engineering: B* **138**, 77 (2007).

- [21] B.E. Sernelius, K.-F. Berggren, Z.-C. Jin, I. Hamberg, C.G. Granqvist, *Physical Review B* **37**, 10244 (1988).
- [22] R.L. Pozzo, M.A. Baltanas, A.E. Cassano, *Catalysis Today* **39**, 231 (1997).
- [23] I. Demir, *Superlattices and Microstructures* **128**, 8 (2019).
- [24] A. Kapıcıoğlu, H. Esen, *E Applied Thermal Engineering* **165**, 114559 (2020).
- [25] H. Demir, Ö. Şahin, O. Baytar, S. Horoz, *Journal of Materials Science: Materials in Electronics* **31**, 10354 (2020).
- [26] X. Qiu, L. Li, J. Zheng, J. Liu, X. Sun, G. Li, *The Journal of Physical Chemistry C* **112**, 12248 (2008).
- [27] C. Abed, M.B. Ali, A. Addad, H. Elhouichet, *Materials Research Bulletin* **110**, 238 (2019).
- [28] O. Baytar, A.A. Ceyhan, Ö. Şahin, *International Journal of Phytoremediation* **23**, 703 (2020).
- [29] Ö. Şahin, A. Ekinci, S. Horoz, *SJournal of Materials Science: Materials in Electronics* **30**, 7605 (2019).
- [30] S.-W. Zhao, H.-F. Zuo, Y.-R. Guo, Q.-J. Pan, *Journal of Alloys and Compounds* **695**, 1037 (2017).
- [31] C. Zörer, O. Baytar, Ö. Şahin, S. Horoz, M. Izgi, *Digest Journal of Nanomaterials & Biostructures (DJNB)* **15**, 636 (2020).
- [32] U. Holzwarth, N. Gibson, *Nature nanotechnology* **6**, 534 (2011).
- [33] A. Tumuluri, K.L. Naidu, K.J. Raju, *B Int. J. ChemTech Res* **6**, 3356 (2014).
- [34] K.R. Reddy, P. Prathap, N. Revathi, A. Reddy, R. Miles, *Thin Solid Films* **518**, 278 (2009).
- [35] V. Srisuvetha, S. Rayar, G. Shanthi, *Journal of Materials Science: Materials in Electronics* **31**, 2808 (2020).